ACSNANO
www.acsnano.org
ARTICLE

Epitaxial Growth of Aligned and Continuous Carbon Nanofibers from Carbon Nanotubes

Xiaoyang Lin,[*,†,‡,§] Wei Zhao,[†,§] Wenbin Zhou,[⊥] Peng Liu,[*,†] Shu Luo,[†] Haoming Wei,[†] Guangzhi Yang,[#] Junhe Yang,[#] Jie Cui,[⊥] Richeng Yu,[⊥] Lina Zhang,[†] Jiaping Wang,[†] Qunqing Li,[†] Weiya Zhou,[⊥] Weisheng Zhao,[‡] Shoushan Fan,[†] and Kaili Jiang[*,†]

[†]State Key Laboratory of Low-Dimensional Quantum Physics, Department of Physics & Tsinghua-Foxconn Nanotechnology Research Center, Collaborative Innovation Center of Quantum Matter, Tsinghua University, Beijing 100084, China
[‡]Fert Beijing Research Institute, School of Electrical and Information Engineering, BDBC, Beihang University, Beijing 100191, China
[⊥]Beijing National Laboratory of Condensed Matter Physics, Institute of Physics, Chinese Academy of Sciences, Beijing 100190, China
[#]School of Materials Science and Engineering, University of Shanghai for Science and Technology, Shanghai 200093, China

Supporting Information

ABSTRACT: **Exploiting the superior properties of nanomaterials at macroscopic scale is a key issue of nanoscience. Different from the integration strategy, "additive synthesis" of macroscopic structures from nanomaterial templates may be a promising choice. In this paper, we report the epitaxial growth of aligned, continuous, and catalyst-free carbon nanofiber thin films from carbon nanotube films. The fabrication process includes thickening of continuous carbon nanotube films by gas-phase pyrolytic carbon deposition and further graphitization of the carbon layer by high-temperature treatment. As-fabricated nanofibers in the film have an "annual ring" cross-section, with a carbon nanotube core and a graphitic periphery, indicating the templated growth mechanism. The absence of a distinct interface between the carbon nanotube template and the graphitic periphery further implies the epitaxial growth mechanism of the fiber. The mechanically robust thin film with tunable fiber diameters from tens of nanometers to several micrometers possesses low density, high electrical conductivity, and high thermal conductivity. Further extension of this fabrication method to enhance carbon nanotube yarns is also demonstrated, resulting in yarns with ~4-fold increased tensile strength and ~10-fold increased Young's modulus. The aligned and continuous features of the films together with their outstanding physical and chemical properties would certainly promote the large-scale applications of carbon nanofibers.**

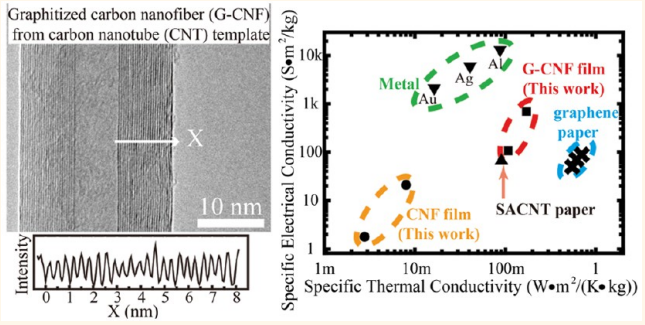

KEYWORDS: *additive synthesis, aligned, continuous, carbon nanofiber, carbon nanotube*

Fibrous carbon or carbon fiber, an important member of the carbon family, together with carbon nanotube (CNT) and graphene, has been envisaged as a key material of green science and technology.[1] Among all forms of carbon fibers, vapor-grown carbon fibers (VGCFs) synthesized with floating catalysts can be a solution for large-scale randomly oriented and discontinuous carbon fibers.[2−4] However, the existence of catalyst residues and the randomly oriented and discontinuous feature of VGCFs have limited their potential applications. A facile method to fabricate well-aligned, continuous, and catalyst-free carbon fibers is thus highly desired for large-scale and high-performance applications of carbon fibers.

The growth process of VGCFs can be divided into two steps: catalytic growth of the CNT core and thickening of the pyrolytic carbon periphery.[2,4] Such a growth mechanism implies the possibility to realize "additive synthesis" of carbon fibers from CNTs, *i.e.*, by depositing pyrolytic carbon on the CNT template. In this sense, the quality and morphology distribution of CNTs would affect the features of as-grown carbon fibers. Among the CNTs, the superaligned carbon nanotube (SACNT) enables continuous spinning of aligned CNT films from the SACNT array.[5−7] In this paper, we report the epitaxial growth of aligned, continuous, and catalyst-free carbon nanofiber films (CNF films) from CNT films. As-fabricated fibers in the film have an "annual ring" cross-section, with a CNT core and a graphitic periphery, indicating the template function of the CNT. The absence of a distinct interface between the CNT template and the graphitic periphery further

Received: July 21, 2016
Accepted: February 6, 2017
Published: February 6, 2017

DOI: 10.1021/acsnano.6b04855
ACS Nano 2017, 11, 1257−1263

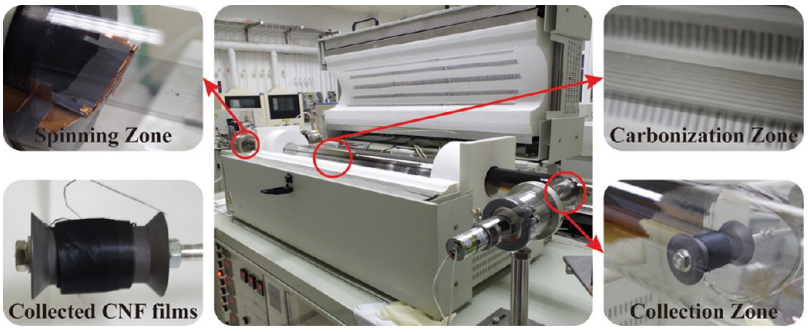

Figure 1. Continuous fabrication of carbon nanofiber films (CNF films) from carbon nanotube films (CNT films). Continuous CNT film is spun from a superaligned carbon nanotube array (SACNT array) fixed at one cold end of the quartz tube (labeled as spinning zone), through the hot zone heated by the furnace (labeled as carbonization zone), to the spool at the other cold end (labeled as collection zone). Pyrolytic carbon is deposited on the CNT due to the pyrolysis of the hydrocarbon gas in the carbonization zone. The collection of CNF films on the spool is driven by a dc motor. (Note that the photograph of the collection zone is mirrored; the width of the CNF films collected on the spool is 3 cm.)

implies the epitaxial growth mechanism of the fiber. The diameter of the fiber, ranging from tens of nanometers to several micronmeters, can be well controlled by the fabrication conditions. The as-fabricated CNF films with low density, good mechanical performance, high electrical conductivity, and high thermal conductivity would meet the demand of lightweight, high-strength, good-conductivity applications. Further extension of the fabrication method to achieve carbon yarns with several-fold-enhanced mechanical performance is also demonstrated.

RESULTS AND DISCUSSION

We start from the CNT film spun from the SACNT array, which acts as a template for pyrolytic carbon deposition and the following graphitization (Figure 1). As shown in Figure 1, continuous fabrication of CNF films was realized in a quartz tube with a tubular furnace. The continuous-spinning feature of the SACNT,[5,6,8] enables the integration of continuous spinning of CNT films from the SACNT array (at one cold end of the quartz tube, "spinning zone" in Figure 1), continuous deposition of pyrolytic carbon on the film (in the hot zone, "carbonization zone" in Figure 1), and continuous collection of the as-grown CNF film (at the other cold end, "collection zone" in Figure 1). The length of the CNFs would only be limited by the size of CNT array used, which can beyond hundreds of meters.[5] The collected CNF films can be continuously spun from the spool, which would benefit further treatments (*e.g.*, high-temperature graphitization treatment for graphitized carbon nanofibers, denoted as G-CNFs) or applications of the film.

The "additive synthesis" strategy from the CNT film template (Figure 2a) endows some characteristics of the CNF and G-CNF film. After the fabrication process, as-grown G-CNFs with an increased diameter (25 nm to 1.6 μm, depending on the carbon deposition time) maintain the well-aligned feature of the parent CNT film (see Figure 2b and c for the CNT film and G-CNF film, respectively). A scanning electron microscopy (SEM) observation on the tip of the fibers indicates an "annual ring" structure of the fiber, with a CNT core and a carbon periphery (Figure 2d), verifying the template function of the CNT.[2,9−11] The "additive synthesis" from the CNT template also ensures the catalyst-free feature of the CNFs and the G-CNFs, which can be supported by the energy-dispersive X-ray spectroscopy (EDS) results (Figure 2e).

More information on the structural feature and also the growth mechanism of the fibers can be given by transmission electron microscope (TEM) characterizations. According to the TEM results, G-CNFs with different diameters all displayed good graphitization, supporting the graphitizable feature of the pyrolytic carbon.[4,12] For G-CNFs with a diameter of about tens of nanometers, the absence of a distinct interface between the CNT template (diameter ~10 nm) and the graphitic periphery implies the epitaxial growth mechanism of the fiber (Figure 3a and the inset and Figure S10). The finding of graphitic structures in small-diameter CNFs without high-temperature treatment (diameter below 100 nm, see Figure S1 for both the side-view and cross-section TEM results) further indicates the potential ability of the CNT template to induce epitaxial graphitization, which is in agreement with previous reports on individual CNTs.[13] Besides the typical spacing (~0.34 nm) between graphitic layers, some additional spacing with a period of around tens of nanometers can also be found in the graphitic periphery of G-CNFs with a sub-micrometer diameter (Figure 3c and Figure S2). Such a phenomenon may be a result of the strain induced by the curvature of the G-CNFs (Figure S3), which would hinder graphitic stacking and induce shape transformations during the growth.[10,14,15] In addition to characterizations of individual G-CNFs, additional attention was paid to the crystalline structure of the G-CNF junctions. A high degree of graphitization was found on the fibers away from the G-CNF junction (Figure S4). As displayed in Figure S4b and d, some multiloops between graphitic layers of two fibers (in two directions) were found in the G-CNF junction. The parent CNTs in the same junction are held together *via* van der Waals interactions. The formation of graphitic loops in the junction would thus contribute to improved mechanical, electrical, and thermal performances of the G-CNF films.

The EDS results (Figure 2e) indicate the all-carbon feature of the CNF film and G-CNF film. Analyses by X-ray photoelectron spectroscopy (XPS) and thermogravimetry (TG) further reveal the sp^2 carbon chemical state and high graphitization of the G-CNF film (Figure S5a,b and Supporting Information). To evaluate the crystalline structure of the fiber, X-ray diffraction (XRD) and Raman analyses were performed on the samples (Figure 4a and b). Compared to the XRD results of the CNF and the CNT film, the sharpest (002) line with the largest diffraction angle can be found in the G-CNF film. According to the Scherrer equation,[16]

DOI: 10.1021/acsnano.6b04855
ACS Nano 2017, 11, 1257−1263

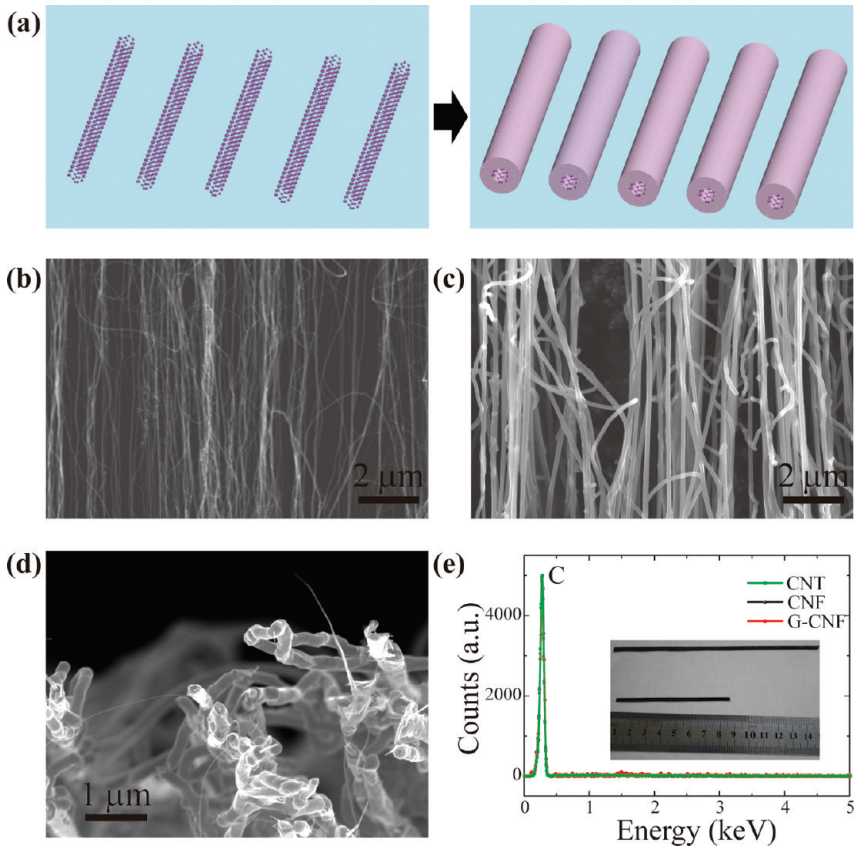

Figure 2. Structural and composition feature of the fiber. (a) Schematic illustration of the structure transformation from the CNT template to the CNFs. (b, c) Scanning electron microscopy (SEM) images of (b) SACNT film and (c) graphitized carbon nanofiber film (G-CNF film). The diameter of the G-CNFs is around 150 nm. (d) SEM image of G-CNFs, focused on the fiber tips. (e) Energy-dispersive X-ray spectroscopy (EDS) results of CNT, CNF, and G-CNF films. Inset is a photograph of G-CNF film strips.

$$L_c = \frac{K\lambda}{\mathrm{FWHM}(2\theta)\cos\theta} \quad (1)$$

(L_c is the crystallite size, K is the Scherrer constant, λ is the wavelength of the X-ray, θ is half of the diffraction angle of the XRD line, and FWHM(2θ) is the full width at half-maximum of the XRD line), such a feature suggests the successful graphitization of the G-CNF by high-temperature treatment. Such a judgment is also confirmed by the Raman results (Figure 4b), which provide local structure information on the sample within the optical skin depth.[14,17] A negligible D peak and a sharp G peak in the spectrum suggest the good crystallinity feature of the G-CNF.[15,18] The differences in the peak intensity ratio I_G/I_D and the width of the G peak between the CNF and the G-CNF identify the effect of the graphitization treatment: to improve the crystallinity of the sample.[1,18−21]

To evaluate the physical properties of the films, effective thicknesses of the CNF films and G-CNF films with different fiber diameters were measured in SEM by clamping the film with two silicon slices (Figure S6, these values may be overestimated considering the measurement method). For CNF and G-CNF films with a similar fiber diameter of 250 nm, the measured thicknesses are 3.2 and 8.3 μm, respectively. Considering the mass density and resistivity results (Figure S7), such a feature is coincident with structure transformations of the periphery in the fiber from amorphous carbon to graphitic carbon.

A similar difference can be found in the mechanical performance. Graphitization treatment results in stiffer G-CNF films compared to the pristine CNF films (Figure 4c−f). Besides, the tensile strength, Young's modulus, and fracture strain results all exhibit some fiber diameter dependence. Both tensile strength and the Young's modulus of the G-CNF film reach maximum values around a diameter of 1 μm. Such a fiber diameter dependence may originate from structure evolutions of the G-CNF film. As the fiber diameter increases, the influence of curvature-induced strain would weaken,[14,15] resulting in more perfect fibers (*i.e.*, improved mechanical performance). However, when the fiber diameter reaches 1 μm, lots of G-CNFs coalesce together and become seamless films covered by loose graphitic layers (Figure S8), which results in poor stress transfer among the embedded G-CNFs during the mechanical test. The highest tensile strength of the G-CNF film (with a fiber diameter ~980 nm) is measured to be 214 ± 42 MPa. The corresponding specific strength is 158 ± 31 MPa/(g/cm^3), which is comparable to or even larger than those of Mylar or Kapton films (~160 MPa/(g/cm^3)) and high-strength steel (~125 MPa/(g/cm^3)).[7] For practical applications in the aerospace industry, lightweight but high-performance materials are highly desired. The continuous G-CNF film is proved to simultaneously possess the features of low density, high electrical conductivity, high mechanical strength, and high thermal conductivity. Rough comparisons among free-standing film/membrane materials with respect to the specific electrical conductivity and specific thermal conductivity (Figure 5) indicate that the G-CNF film can be a solution for lightweight, high electrical/thermal conductivity materials.

DOI: 10.1021/acsnano.6b04855
ACS Nano 2017, 11, 1257−1263

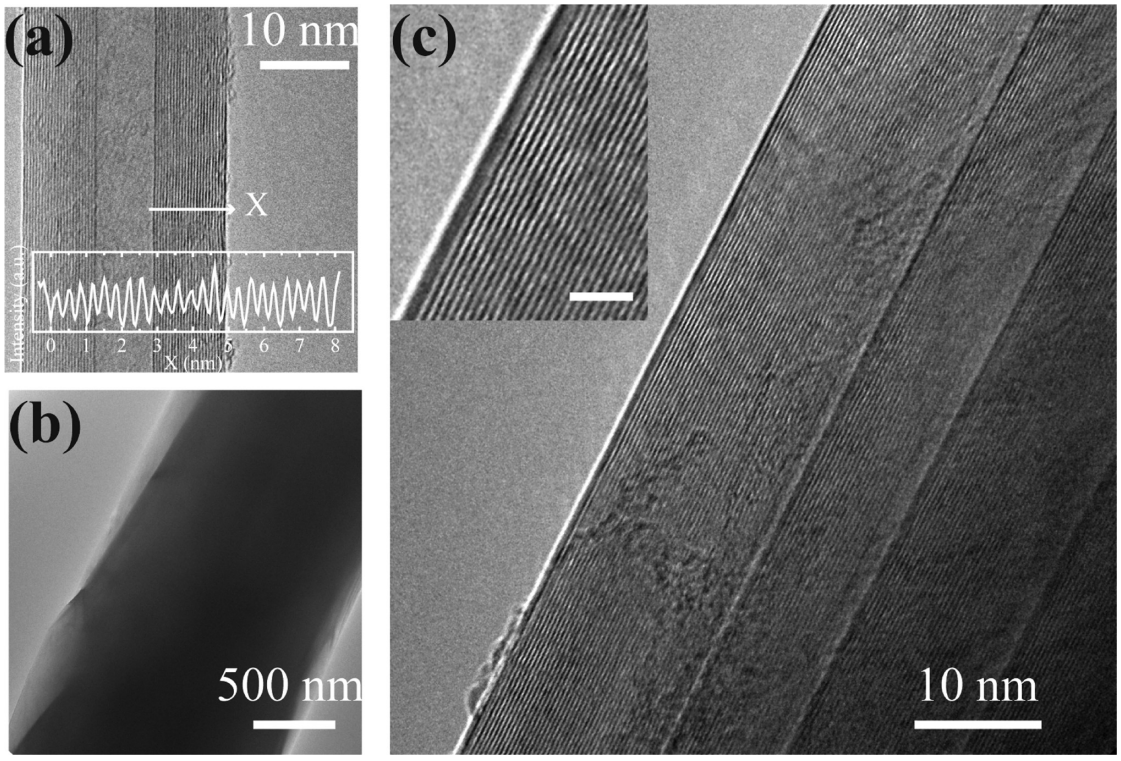

Figure 3. Transmission electron microscopy (TEM) images of G-CNFs. (a) TEM image of a G-CNF with a diameter around 30 nm. The inset shows the contrast profile along the marked line in (a). (b, c) TEM images of a G-CNF with a diameter around 1.6 μm. The inset of (c) shows the crystalline structure of the fiber; the scale bar is 2.5 nm.

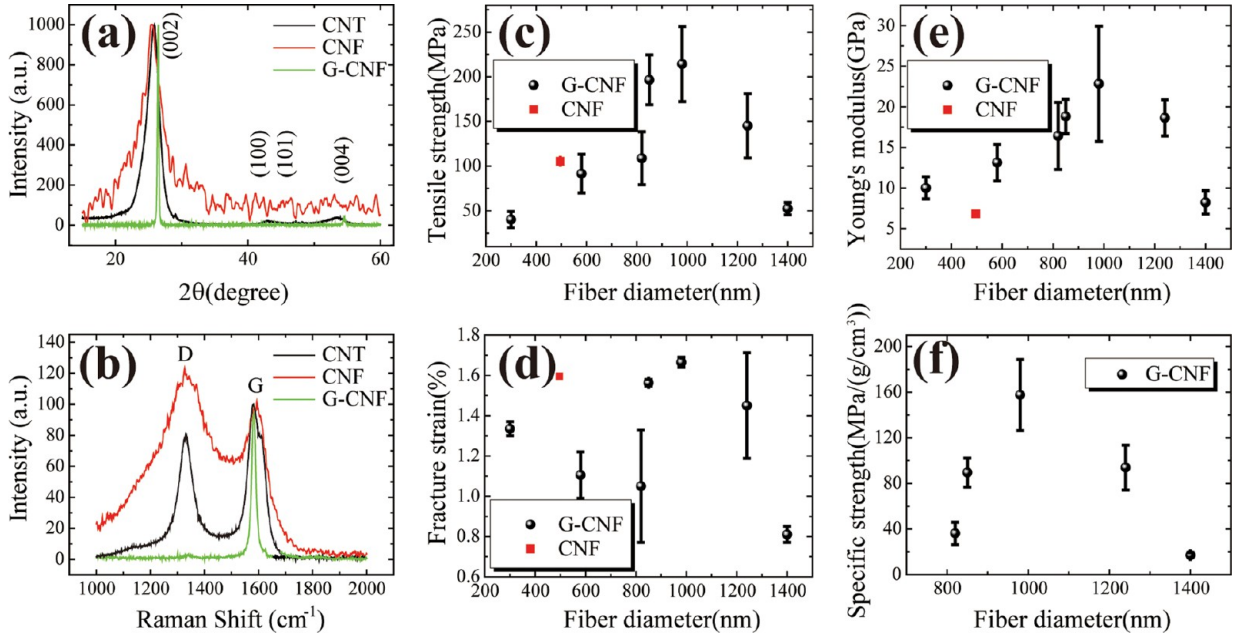

Figure 4. Characterizations and mechanical performance of the CNT, CNF, and G-CNF films. (a) X-ray diffraction (XRD) results of CNT, CNF, and G-CNF films. (b) Raman results of CNT films, CNFs, and G-CNFs. (c–f) Fiber diameter dependence of the tensile strength (c), fracture strain (d), Young's modulus (e), and specific strength (f) of the G-CNFs and CNFs.

One feature of the G-CNF is the diameter-dependent crystallinity. As shown in Table S1, Raman and XRD data are processed and summarized into some graphitization indices as a function of fiber diameter. Since the existence of defects in the G-CNF would cause both intensity change and broadening of the Raman peak,[18−21] values of average in-plane graphene length (L_a) and average graphene length including curvature (L_{eq}) of the fiber can be evaluated according to the integrated intensity ratio of Raman peaks as $L_a \propto A_G/A_D$ and $L_{eq} \propto A_{2D}/A_D$.[20,22] The ratio $L_{eq}/L_a \propto A_{2D}/A_G$ would thus provide information about the curvature in the G-CNF. The summarized results that a fiber with a larger diameter substantially has larger values of A_G/A_D and A_{2D}/A_D, but a smaller A_{2D}/A_G (Table S1) indicate a positive correlation between fiber diameter and the

DOI: 10.1021/acsnano.6b04855
ACS Nano 2017, 11, 1257−1263

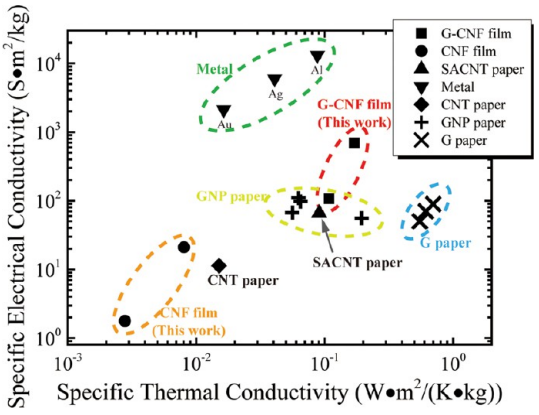

Figure 5. Comparisons of free-standing film/membrane materials with respect to their specific electrical conductivity and specific thermal conductivity. The materials include G-CNF film (fiber diameter ~980 and 280 nm), CNF film (fiber diameter ~2400 and 265 nm), and 10-layered SACNT film (SACNT paper), together with some metals (Au, Ag, Al, see ref 25), CNT bucky paper (denoted as CNT Paper, see ref 26.), graphene nanoplatelet paper (GNP paper, see ref 26), and graphene paper (G paper, see ref 27).

graphitization. Different from the spatially localized characterization by Raman,[14,17] XRD analysis can perform crystallinity characterization within a much larger area (~600 μm in diameter). The *c*-axis interlayer spacing (d_{002}), the degree of graphitization (G), and crystallite size along the *c*-axis (L_c(002), calculated by eq 1) are three graphitization indices for evaluating the crystallinity of the G-CNFs (see Supporting Information for calculation details). The range of the L_c(002) (21.5–34.8 nm) is roughly in agreement with the period of the extra spacing observed in TEM (Figure 3c). The d_{002} and G% of G-CNFs with different diameters distribute within 0.3368–0.3391 nm and 54.6–79.6%, respectively. Deviations of the values from those of the perfect graphite (d_{002} = 0.335 nm and G% = 100%) can be explained by the existence of curvature and multiloops (between graphitic layers, Figure S4) in the G-CNFs.[14,15] The diameter dependence of these indices once again demonstrates the positive correlation between fiber diameter and the graphitization, verifying the effect of curvature to hinder perfect graphitization in the fiber.

The "additive synthesis" method can also be applied to fabricate mechanically enhanced carbon yarns from a CNT yarn template. CNT yarns with different diameters can be achieved by shrinking SACNT films with specific widths.[23] From these CNT yarn templates, pyrolytic carbon coated CNT yarns (C-yarns) and graphitized C-yarns (G-C-yarns) can be prepared using the aforementioned method. As a demo, carbon yarns with a 6.5 μm diameter and 100 nm thick carbon or graphite layer were fabricated and tested. The mechanical test results (Figure 6a and b) indicate a "stiffer" feature of the G-C-yarn (tensile strength 0.6 ± 0.3 GPa, Young's modulus 219.2 ± 80.8 GPa) and a "stronger" feature of the C-yarn (tensile strength 1.6 ± 1.4 GPa, Young's modulus 91.2 ± 80.4 GPa). Compared to the pristine CNT yarn (tensile strength 0.4 ± 0.2 GPa, Young's modulus 18.6 ± 8.9 GPa), the greatly improved mechanical performance (~4-fold increased tensile strength for C-yarn, ~10-fold increased Young's modulus for G-C-yarn) can be explained by the effective stress transfer among the CNTs in the yarn due to the existence of carbon or graphitic periphery layers (Figure 6d). The well-improved mechanical performance, together with the continuous feature of the CNT yarn, makes such a method appealing for versatile applications of CNT yarns.

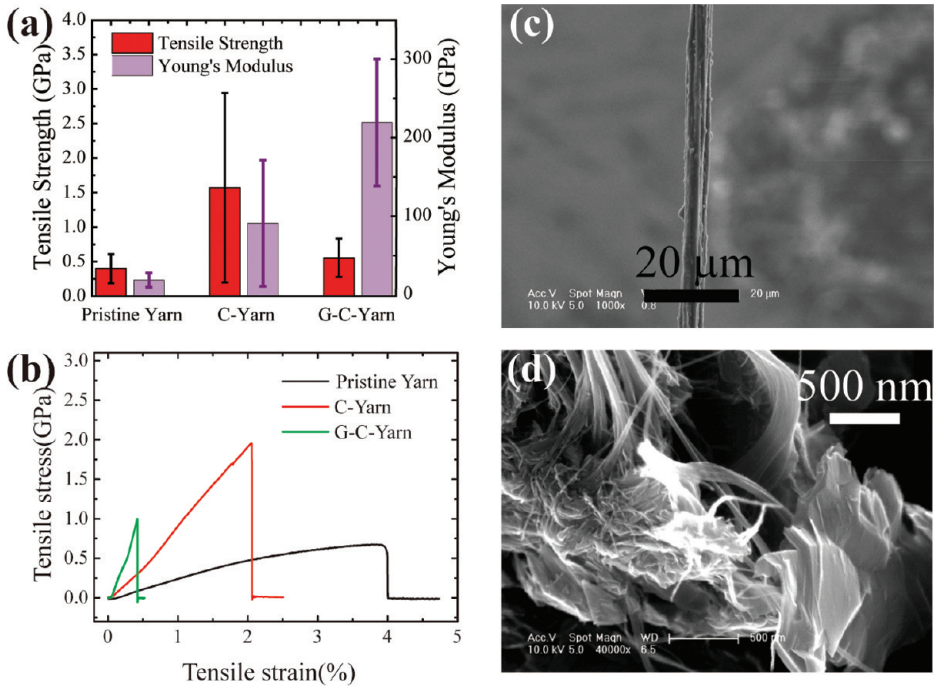

Figure 6. Applications of the "additive synthesis" method. (a) Statistical results of the tensile strength and Young's modulus of pristine CNT yarns (labeled as "pristine yarn"), pyrolytic carbon coated CNT yarns (labeled as "C-yarn"), and further graphitization-treated CNT yarns (labeled as "G-C-yarn"), all with diameters around 6.5 μm. (b) Typical stress–strain curves of pristine yarn, C-yarn, and G-C-yarn with diameters around 6.5 μm. (c) SEM image of the CNT yarns after pyrolytic carbon deposition and high-temperature graphitization treatment. (d) Cross-section SEM image of the yarn in (c).

DOI: 10.1021/acsnano.6b04855
ACS Nano 2017, 11, 1257–1263

CONCLUSION

In summary, we have realized "additive synthesis" of continuous, aligned, catalyst-free carbon/graphitic nanofiber films from the carbon nanotube film template. The fabrication process includes pyrolytic carbon deposition on the carbon nanotube film template and graphitization treatment of the film. Such a two-step fabrication method results in an "annual ring" structure of the fiber, just like a tree. The "annual ring" cross-section of the fiber, together with the absence of a distinct interface between the carbon nanotube template and the graphitic periphery, implies the epitaxial growth mechanism of the fiber. The continuous carbon/graphitic nanofiber films, with merits of good alignment, low weight, high mechanical performance, good electrical conductivity, and good thermal conductivity, would certainly promote the large-scale application of carbon nanofibers.

METHODS

Fabrications of the Fiber. For discontinuous fabrication of CNF films, the as-spun CNT film was first support by a graphite frame with a suspending size of 40 mm × 15 mm. Pyrolytic carbon deposition was then performed *via* pyrolysis of hydrocarbon gas (50 mL/min CH_4 diluted by 50 mL/min Ar) at 1050 °C for 1−40 min in a quartz tube (22 mm inner diameter) with a hot-wall furnace (Lindberg Blue M TF55035C-1). For continuous fabrication of CNF films, spinning of CNT films from the SACNT array, pyrolytic carbon deposition, and CNF film collection were all integrated inside a quartz tube (70 mm inner diameter) with a hot-wall furnace (Lindberg Blue M HTF55667C), as shown in Figure 1. To get the G-CNF film, the CNF film was further graphitized in an Ar atmosphere at a temperature around 2900 °C for 1 h using a graphitization furnace (KGPS-100, ChenXin Induction Equipment Co., Ltd.).

Characterizations and Measurements. SEM (FEI Sirion 200), TEM (FEI Tecnai G2 F20 S-Twin), XRD (Rigaku D/max 2500PC), and Raman spectroscopy (Jobin Yvon LabRAM HR800) were used to characterize the samples. The mechanical test was performed using an Instron 5848 MicroTester. The measurements of in-plane thermal conductivity were performed by a self-heating method using a homemade apparatus. To improve the accuracy of the measurement, (1) the measurement was performed in a vacuum of ~1×10^{-3} Pa; (2) thin film strips with large ratio of length to width were prepared to meet the demand of one-dimensional thermal conduction; and (3) radiant heat loss was taken into account when calculating the thermal conductivity. More information on the method can be found in a previous paper.[24]

ASSOCIATED CONTENT

Supporting Information

The Supporting Information is available free of charge on the ACS Publications website at DOI: 10.1021/acsnano.6b04855.

Structural characterizations and analyses of the fibers, effective thickness measurements of the films, and SEM images of G-CNF films with different fiber diameters (PDF)

AUTHOR INFORMATION

Corresponding Authors

*E-mail: XYLin@buaa.edu.cn (X.-Y. Lin).
*E-mail: pengliu@tsinghua.edu.cn (P. Liu).
*E-mail: JiangKL@tsinghua.edu.cn (K.-L. Jiang).

ORCID

Peng Liu: 0000-0002-1860-5126
Richeng Yu: 0000-0002-8086-0910

Author Contributions

§X.-Y. Lin and W. Zhao contributed equally to this work.

Notes

The authors declare no competing financial interest.

ACKNOWLEDGMENTS

The work was funded by the National Basic Research Program of China (2012CB932300), the NSFC (11274190, 51602013, 51672152, and 51472142), and the Beijing Natural Science Foundation (4162039). The authors would like to thank Mr. Penghan Lu, Prof. Zhi-Wei Shan, and Prof. Yuan Yao for their help during the TEM characterization.

REFERENCES

(1) Kim, Y. A.; Hayashi, T.; Endo, M.; Dresselhaus, M. S. Carbon Nanofibers. In *Springer Handbook of Nanomaterials*; Vajtai, R., Ed.; Springer, 2013; pp 233−262.
(2) Endo, M. Grow Carbon Fibers in the Vapor Phase. *CHEMTECH* **1988**, *18*, 568−576.
(3) Tibbetts, G. G. Why are Carbon Filaments Tubular? *J. Cryst. Growth* **1984**, *66*, 632−638.
(4) Oberlin, A.; Endo, M.; Koyama, T. Filamentous Growth of Carbon through Benzene Decomposition. *J. Cryst. Growth* **1976**, *32*, 335−349.
(5) Jiang, K. L.; Wang, J. P.; Li, Q. Q.; Liu, L. A.; Liu, C. H.; Fan, S. S. Superaligned Carbon Nanotube Arrays, Films, and Yarns: A Road to Applications. *Adv. Mater.* **2011**, *23*, 1154−1161.
(6) Jiang, K. L.; Li, Q. Q.; Fan, S. S. Nanotechnology: Spinning Continuous Carbon Nanotube Yarns - Carbon Nanotubes Weave their Way into a Range of Imaginative Macroscopic Applications. *Nature* **2002**, *419*, 801.
(7) Zhang, M.; Fang, S. L.; Zakhidov, A. A.; Lee, S. B.; Aliev, A. E.; Williams, C. D.; Atkinson, K. R.; Baughman, R. H. Strong, Transparent, Multifunctional, Carbon Nanotube Sheets. *Science* **2005**, *309*, 1215−1219.
(8) Liu, K.; Sun, Y. H.; Chen, L.; Feng, C.; Feng, X. F.; Jiang, K. L.; Zhao, Y. G.; Fan, S. S. Controlled Growth of Super-Aligned Carbon Nanotube Arrays for Spinning Continuous Unidirectional Sheets with Tunable Physical Properties. *Nano Lett.* **2008**, *8*, 700−705.
(9) Tibbetts, G. G. Vapor-Grown Carbon Fibers: Status and Prospects. *Carbon* **1989**, *27*, 745−747.
(10) Speck, J. S.; Endo, M.; Dresselhaus, M. S. Structure and Intercalation of Thin Benzene Derived Carbon Fibers. *J. Cryst. Growth* **1989**, *94*, 834−848.
(11) Endo, M.; Takeuchi, K.; Kobori, K.; Takahashi, K.; Kroto, H. W.; Sarkar, A. Pyrolytic Carbon Nanotubes from Vapor-Grown Carbon Fibers. *Carbon* **1995**, *33*, 873−881.
(12) Endo, M.; Kim, Y. A.; Hayashi, T.; Nishimura, K.; Matusita, T.; Miyashita, K.; Dresselhaus, M. S. Vapor-Grown Carbon Fibers (VGCFs) - Basic Properties and their Battery Applications. *Carbon* **2001**, *39*, 1287−1297.
(13) Feng, X.; Liu, K.; Xie, X.; Zhou, R.; Zhang, L.; Li, Q.; Fan, S.; Jiang, K. Thermal Analysis Study of the Growth Kinetics of Carbon Nanotubes and Epitaxial Graphene Layers on them. *J. Phys. Chem. C* **2009**, *113*, 9623−9631.
(14) Endo, M.; Kim, Y. A.; Takeda, T.; Hong, S. H.; Matusita, T.; Hayashi, T.; Dresselhaus, M. S. Structural Characterization of Carbon Nanofibers Obtained by Hydrocarbon Pyrolysis. *Carbon* **2001**, *39*, 2003−2010.
(15) Endo, M.; Nishimura, K.; Kim, Y. A.; Hakamada, K.; Matushita, T.; Dresselhaus, M. S.; Dresselhaus, G. Raman Spectroscopic Characterization of Submicron Vapor-Grown Carbon Fibers and Carbon Nanofibers Obtained by Pyrolyzing Hydrocarbons. *J. Mater. Res.* **1999**, *14*, 4474−4477.
(16) Scherrer, P. Bestimmung Der Grösse Und Der Inneren Struktur Von Kolloidteilchen Mittels Röntgenstrahlen. *Nachr. Ges. Wiss. Goettingen, Math.-Phys. Kl.* **1918**, *1918*, 98−100.

DOI: 10.1021/acsnano.6b04855
ACS Nano 2017, 11, 1257−1263

(17) Baddour-Hadjean, R.; Pereira-Ramos, J. Raman Microspectrometry Applied to the Study of Electrode Materials for Lithium Batteries. *Chem. Rev.* **2010**, *110*, 1278−1319.
(18) Ferrari, A. C. Raman Spectroscopy of Graphene and Graphite: Disorder, Electron-Phonon Coupling, Doping and Nonadiabatic Effects. *Solid State Commun.* **2007**, *143*, 47−57.
(19) Lespade, P.; Marchand, A.; Couzi, M.; Cruege, F. Caracterisation De Materiaux Carbones Par Microspectrometrie Raman. *Carbon* **1984**, *22*, 375−385.
(20) Larouche, N.; Stansfield, B. L. Classifying Nanostructured Carbons Using Graphitic Indices Derived from Raman Spectra. *Carbon* **2010**, *48*, 620−629.
(21) Lespade, P.; Al-Jishi, R.; Dresselhaus, M. S. Model for Raman Scattering from Incompletely Graphitized Carbons. *Carbon* **1982**, *20*, 427−431.
(22) Cançado, L. G.; Takai, K.; Enoki, T.; Endo, M.; Kim, Y. A.; Mizusaki, H.; Jorio, A.; Coelho, L. N.; Magalhaes-Paniago, R.; Pimenta, M. A. General Equation for the Determination of the Crystallite Size L_a of Nanographite by Raman Spectroscopy. *Appl. Phys. Lett.* **2006**, *88*, 163106.
(23) Wei, Y.; Liu, P.; Jiang, K.; Fan, S. A Display Module Implemented by the Fast High-Temperature Response of Carbon Nanotube Thin Yarns. *Nano Lett.* **2012**, *12*, 2548−2553.
(24) Zhou, W.; Fan, Q.; Zhang, Q.; Li, K.; Cai, L.; Gu, X.; Yang, F.; Zhang, N.; Xiao, Z.; Chen, H.; Xiao, S.; Wang, Y.; Liu, H.; Zhou, W.; Xie, S. Ultrahigh-Power-Factor Carbon Nanotubes and an Ingenious Strategy for Thermoelectric Performance Evaluation. *Small* **2016**, *12*, 3407−3414.
(25) Berger, L. I. *CRC Handbook of Chemistry and Physics*, 96 ed.; CRC Press/Taylor and Francis: Boca Raton, FL, 2016.
(26) Wu, H.; Drzal, L. T. Graphene Nanoplatelet Paper as a Light-Weight Composite with Excellent Electrical and Thermal Conductivity and Good Gas Barrier Properties. *Carbon* **2012**, *50*, 1135−1145.
(27) Xin, G.; Sun, H.; Hu, T.; Fard, H. R.; Sun, X.; Koratkar, N.; Borca-Tasciuc, T.; Lian, J. Large-Area Freestanding Graphene Paper for Superior Thermal Management. *Adv. Mater.* **2014**, *26*, 4521−4526.

DOI: 10.1021/acsnano.6b04855
ACS Nano 2017, 11, 1257−1263